

## Cortical thickness measured from MRI in the YAC128 mouse model of Huntington's disease

Jason P. Lerch,<sup>a,\*</sup> Jeffrey B. Carroll,<sup>b</sup> Adrienne Dorr,<sup>c</sup> Shoshana Spring,<sup>a</sup> Alan C. Evans,<sup>d</sup> Michael R. Hayden,<sup>c</sup> John G. Sled,<sup>a</sup> and R. Mark Henkelman<sup>a</sup>

<sup>a</sup>The Mouse Imaging Centre, The Hospital for Sick Children, Toronto, Ontario, Canada

<sup>b</sup>Centre for Molecular Medicine and Therapeutics, Child and Family Research Institute, Department of Neuroscience, University of British Columbia, Vancouver, British Columbia, Canada

<sup>c</sup>Centre for Molecular Medicine and Therapeutics, Child and Family Research Institute, Department of Medical Genetics, University of British Columbia, Vancouver, British Columbia, Canada

<sup>d</sup>Montreal Neurological Institute, McGill University, Montreal, Quebec, Canada

<sup>e</sup>Clinical Integrative Biology, Sunnybrook Health Sciences Centre, Toronto, Ontario, Canada

Received 16 August 2007; revised 16 January 2008; accepted 7 February 2008  
Available online 26 February 2008

**A recent study found differences in localised regions of the cortex between the YAC128 mouse model of Huntington's Disease (HD) and wild-type mice. There are, however, few tools to automatically examine shape differences in the cortices of mice. This paper describes an algorithm for automatically measuring cortical thickness across the entire cortex from MRI of fixed mouse brain specimens. An analysis of the variance of the method showed that, on average, a 50  $\mu\text{m}$  (0.05 mm) localised difference in cortical thickness can be measured using MR scans. Applying these methods to 8-month-old YAC128 mouse model mice representing an early stage of HD, we found an increase in cortical thickness in the sensorimotor cortex, and also revealed regions wherein decreasing striatal volume correlated with increasing cortical thickness, indicating a potential compensatory response.**

© 2008 Elsevier Inc. All rights reserved.

### Introduction

A recent study by our group examined differences between the YAC128 mouse model of Huntington's Disease (HD) and wild-type mice using deformation-based analyses of high-resolution post-mortem MR scans (Lerch et al., 2008). Along with the shrinkage of the striatum (Vonsattel et al., 1985), we found a volume increase in the sensorimotor cortex, a finding mirrored by a study showing that prodromal human HD also features increased cortical thickness (Paulsen et al., 2006) and exhibits compensatory functional responses in the thalamocortical circuit (Feigin et al., 2006).

The tools to investigate shape changes in the mouse cortex are, however, still limited. Histology and stereology-based techniques, while extremely powerful and capable of providing cellular level detail, are labour intensive and thus do not easily produce whole cortex coverage. They are also subject to tissue shrinkage and distortion from sectioning.

MR-based assessment of murine brain shape has recently gained increasing traction (Badea et al., 2007; Pitiot et al., 2007; Ma et al., 2005). The dominant methodology involves automated non-linear alignment of all examined mice towards a common space and is followed by either statistical analyses of the deformation fields or mapping an anatomical atlas back to each animal to measure structure volumes (Ma et al., 2005; Kovacevic et al., 2005; Chen et al., 2006). Among anatomical measurements, the thickness of the cortex in particular is endowed with biological significance, given that this measure can approximate the path taken by the cortical column, the prime computational unit of the cerebral cortex.

The last decade has produced a field of research based on accurately extracting shape models of the human cortex from MR images. As these techniques have become more sophisticated, intriguing new insights into the anatomy of the cortex have been gained, including mapping the pattern of thickening and thinning during development (Sowell et al., 2004) and ageing (Salat et al., 2004), in degenerative (Lerch et al., 2005) and psychiatric disorders (Shaw et al., 2006b), and in relationships between anatomy and behaviour (Shaw et al., 2006a; Walhovd et al., 2006).

Algorithms to measure cortical thickness from MRI follow one of four prototypes. The simplest, and rarest due to the labour intensive nature of the task, are manual measures using the digital equivalent of callipers (Ross et al., 2001; Meyer et al., 1996). A second set of methods which has gained increasing prominence involves the extraction of the inner and outer cortical surfaces using deformable models (MacDonald et al., 2000; Fischl and

\* Corresponding author.

E-mail address: jason@bic.mni.mcgill.ca (J.P. Lerch).

Available online on ScienceDirect (www.sciencedirect.com).

Dale, 2000; Kim et al., 2005). A third set of methods works without explicit polyhedral models, instead computing image boundaries to find the cortex then measuring the thickness of the cortex at the voxel level (Jones et al., 2000; Preul et al., 2005). The last type involves a mix of explicit surface parameterisation and voxel-based cortical thickness methods (Thompson et al., 2005; Miller et al., 2000).

The human cortex is convoluted with the folding pattern differing considerably between individuals. The mouse cortex, on the other hand, is lissencephalic and, given the similarities within inbred strains, almost identical among individuals. This key difference between mice and humans simplifies the creation of a cortical thickness algorithm considerably:

1. The complex deformable model process employed to map the convoluted human cortex is not necessary for the mouse.
2. The similarity across animals allows for near perfect image registration, a task still impossible within human populations.
3. The ability to compute accurate registrations implies that the definition of the cortex and its boundaries can be created by mapping a pre-existing atlas to each animal.

These points suggest that a volume-based cortical thickness algorithm with boundary definitions gained from registration towards an anatomical atlas will be the easiest solution. Explicit surface parameterisation does, however, provide one key advantage: the creation of a surface coordinate system with a controllable number of nodes. Rather than comparing cortical thickness at every voxel, thickness statistics can instead be computed on a much smaller set of vertices over the cortical surface, leading to obvious advantages in controlling for multiple comparisons. Moreover, it allows the data to be smoothed along the manifold, an anatomically more sensible operation than using volumetric Gaussian kernels. A combined method, using voxel-based cortical thickness measures together with a surface coordinate system, suggests itself as an ideal choice of algorithm. It has the further advantage that every voxel in the cortex is part of a path between the inner and outer cortical surface.

The goal of this study, motivated by the intriguing finding of shape differences in the YAC128 Huntington Disease model mice as well as the lack of available tools to investigate the mouse cortex, is to design a framework for automatically measuring cortical thickness from mouse MRI and to use these new tools to further investigate the YAC128 mouse model. These new methods encompass a combination of mouse registration algorithms with adaptations of tools designed to measure cortical thickness from human MRI scans.

## Methods

The proposed method estimates the thickness of the entire cortical manifold. The basic procedure used follows: (1) MRIs of all mice in the study are acquired. (2) A model independent consensus representation of all mice in the study is created using linear and non-linear registration techniques. (3) A previously existing atlas with an associated segmentation of the cortex is then mapped to the result of step 2. (4) The remapped cortical boundaries are then in turn mapped to each of the individual mice. (5) The thickness of the cortex is estimated. (6) Statistics on the population are then computed to determine the relationship between cortical thickness and the covariates of interest.

## Specimen preparation and MR acquisition

The mice were anaesthetised with a combination of Ketamine (100 mg/kg) and Rompun (20 mg/kg) via intraperitoneal injection. A previously described sample preparation protocol for scanning was used with slight modifications (Tyszka et al., 2006). Thoracic cavities were opened and animals were perfused through the left ventricle with 30 mL of phosphate-buffered saline (PBS) (pH 7.4) at room temperature (25 °C). This was followed by infusion with 30 mL of iced 4% paraformaldehyde (PFA) in PBS. Following perfusion, the heads were removed along with the skin, lower jaw, ears and the cartilaginous nose tip. The remaining skull structures containing the brain were allowed to postfix in 4% PFA at 4 °C for 12 h. Following an incubation period of 5 days in PBS and 0.01% sodium azide at 15 °C, the skulls were transferred to a PBS and 2 mM ProHance® (Bracco Diagnostics Inc., Princeton, NJ) solution for at least 7 days at 15 °C. MR imaging occurred 12 to 21 days post-mortem.

A multi-channel 7.0 Tesla MRI scanner (Varian Inc., Palo Alto, CA) with a 6-cm inner bore diameter insert gradient set was used to acquire anatomical images of brains within skulls. Prior to imaging, the samples were removed from the contrast agent solution, blotted and placed into 13 mm diameter plastic tubes filled with a proton-free susceptibility-matching fluid (Fluorinert FC-77, 3M Corp., St. Paul, MN). Three custom-built, 14 mm diameter solenoid coils with a length of 18.3 mm and over wound ends were used to image three brains in parallel. Parameters used in the scans were optimised for grey/white matter contrast: a T2-weighted, 3-D fast spin-echo sequence, with TR/TE=325/32 ms, four averages, field-of-view of 12×12×25 mm and matrix size=432×432×780 giving an image with 0.032 mm isotropic voxels. Total imaging time was 11.3 h. Geometric distortion due to position of the three coils inside the magnet and gradient was corrected using a calibrated MR phantom (Henkelman et al., 2006).

## Model-independent average creation and cortex segmentation

An unbiased model independent average of the MR scans is created through the following procedure (Kovacevic et al., 2005; Chen et al., 2006). All scans are linearly (3 rotations, 3 translations) registered towards a pre-existing atlas based on 20 male and 20 female adult C57Bl/6 mice (Spring et al., 2007), freely available at [www.mouseimaging.ca](http://www.mouseimaging.ca). All possible pairwise 12 parameter registrations (3 scales, 3 shears, 3 rotations, 3 translations) are then computed, and a transform is created for each mouse through matrix averaging. After intensity averaging all transformed scans to create the first population average, representing the average anatomy of the study sample after accounting for overall brain-size differences, an iterative 6 generation multi-scale non-linear alignment procedure is begun, initially registering each mouse towards the 12 parameter registration average, and subsequently towards the average determined from the previous non-linear generation. All registrations are performed using the `mni_autoreg` tools (Collins et al., 1995, 1994), which use an elastic registration algorithm. The end-result is to have all scans in the study deformed into a common space in an unbiased fashion.

The cortical labels were created on an average atlas of 20 male and 20 female 12-week-old C57Bl/6 mice (Spring et al., 2007). The cerebral cortex was manually segmented using the software package Display (<http://www.bic.mni.mcgill.ca/software/Display/Display.html>, Montreal Neurological Institute, Montreal, Canada). Segmentation was performed slice by slice along the coronal orientation;

horizontal and sagittal orientations were used as guidance and all three orientations were needed for manual correction. Careful delineation of the cortex from surrounding structures was performed with the visual aid of online mouse brain histological atlases such as the Allen Reference Atlas (Lein et al., 2007) and the High Resolution Mouse Brain Atlas <http://www.hms.harvard.edu/research/brain/atlas.html> (based on Sidman et al., 1971) as well as a book-based histological atlas (Paxinos and Franklin, 2001).

The male–female average is then non-linearly aligned to the population average under investigation, and the cortex segmentation resampled into the space of the population average. The segmented cortex is then backpropagated along either the inverse final non-linear transform from each mouse or the concatenation of the inverse non-linear transform plus the inverse 12 parameter transform. The former is chosen if overall brain sizes are to be held constant, the latter if cortical thickness is to be measured without any overall scaling of the brains.

The whole procedure for generating a cortical thickness map for each mouse can be seen in Fig. 1. The first steps involve placing the

segmentation of the cerebral cortex into the space of each mouse so that cortical thickness estimates can be computed (Figs. 1a, b). The polygonal surface defining the cortex on the atlas is transformed to each individual mouse, and the annotation of inside, outside and resistant boundary (see section 2.3 for an explanation of the boundaries) is stored on a rasterized grid that is transformed along with the cortical surface. The exact algorithm is the following: The definition of the cortex, and inside, outside and resistant boundaries is stored independently in the space of the atlas. They are concurrently transformed into the space of each mouse. Following the transformation, the polygonal surface defining the cortex is rasterized by a line-scanning algorithm. The transformed boundaries are then blurred with 0.5 mm Gaussian kernel. The rasterized grid necessary to solve Laplace's equation for each mouse is then reconstituted as follows: each voxel is labelled as cortex if it is inside the transformed and rasterized cortex, otherwise it is assigned the label of the inside, outside or resistant boundary depending on which of the three blurred boundary maps had the maximum value at that voxel.

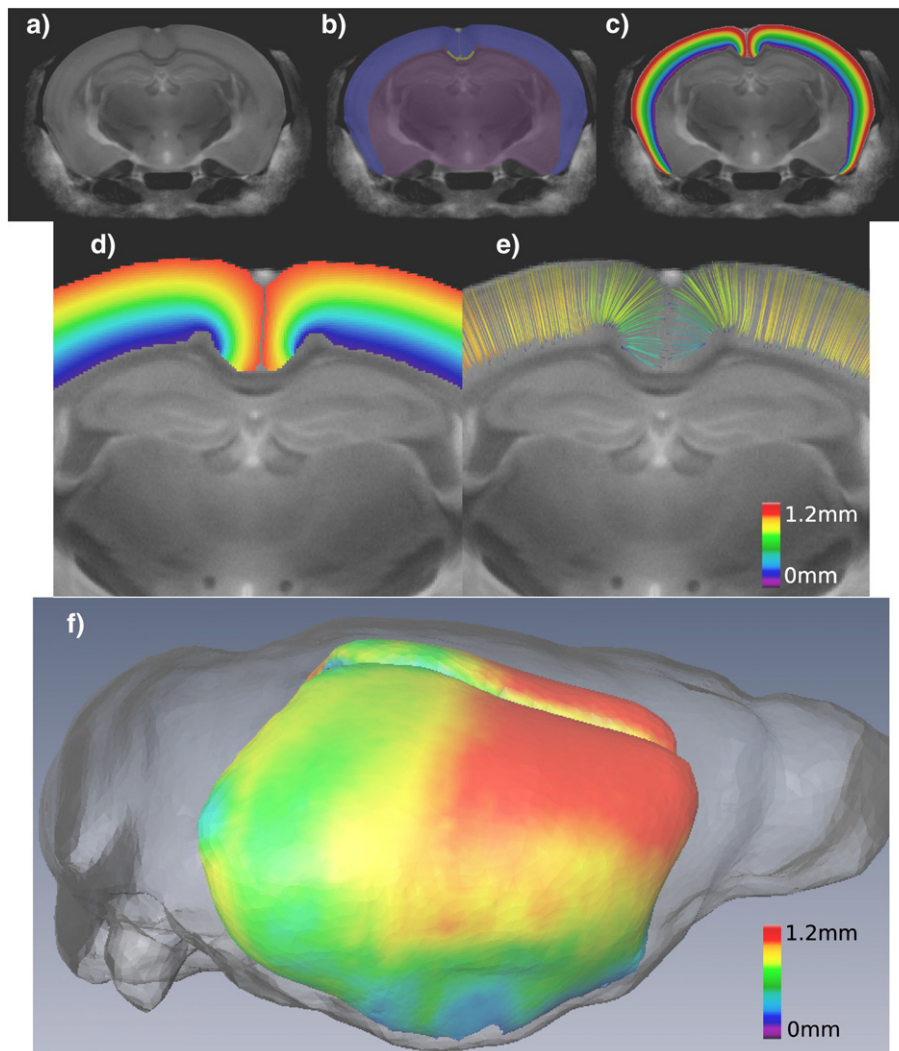


Fig. 1. Measuring cortical thickness. Each MR scan (a) has the segmented cortex mapped to it (b), the blue voxels representing the cortex, the purple voxels the inside boundary, the white voxels the resistive boundary and the remainder the outside boundary. Laplace's equation is then used to create a smooth field between the inside and outside boundaries (c). (d) shows a zoomed view of the potential field around the interhemispheric fissure, and (e) shows the streamlines traversing from the inside boundary to the outside boundary, colour coded according to their length (i.e. thickness). (f) displays the entire cortical thickness mapped on to a manifold.

### Laplacian thickness

The technique for estimating cortical thickness is adapted from Jones et al. (2000), wherein Laplace's Equation is used to create streamlines between the inside and outside cortical surfaces, and the length of these streamlines is used to measure thickness. The entire thickness estimation procedure is illustrated in Fig. 1. Laplace's Equation is a second order partial differential equation for a scalar field  $\psi$  enclosed between two surfaces  $S$  and  $S'$ . It takes the form:

$$\nabla^2\psi = \frac{\partial^2\psi}{\partial x^2} + \frac{\partial^2\psi}{\partial y^2} + \frac{\partial^2\psi}{\partial z^2}$$

In the original paper, three regions were defined: the cortex, the inside boundary and the outside boundary. The anatomical analogy is the path taken by the cortical column, crossing perpendicular to the cortical layers. The algorithm, taken from Jones et al. (2000), follows:

1. The definition of cortex and the boundaries is mapped to each mouse brain via the inverse registration procedure described above.
2. Laplace's equation is iteratively solved using the Jacobi method, keeping the boundaries fixed.
3. Gradients of  $\psi$  are computed using simple two point differences.
4. Streamlines are computed at every voxel by integrating the tangent vector field using Euler's method.

The same scheme is used for the mouse brain. A third, resistive, boundary is added near the interhemispheric fissure. The standard two boundary approach results in all potential lines terminating where the inside and outside boundaries meet, which breaks the analogy to cortical layers (see Fig. 2). The standard two boundaries Jacobian relaxation takes the following form:

$$\psi_{i+1}(x,y,z) = [\psi_i(x+\Delta x,y,z) + \psi_i(x-\Delta x,y,z) + \psi_i(x,y+\Delta y,z) + \psi_i(x,y-\Delta y,z) + \psi_i(x,y,z+\Delta z) + \psi_i(x,y,z-\Delta z)]/6$$

Where  $\psi_{i+1}(x,y,z)$  is the value of the potential at  $x,y,z$  in the  $i$ th iteration. The third boundary modifies the above algorithm slightly. Each condition is checked for whether it is inside the resistive boundary, and if it is, it is not included in the modification of  $\psi_{i+1}(x,y,z)$ , and the denominator is decreased by one. For the majority of the cortex without the resistive boundary present, the algorithm is equivalent to that used in Jones et al. (2000).

### Surface coordinate system

A surface coordinate system is used to compare cortical thickness across a population of mice. The following procedure is used:

1. The laplacian potential field is generated on the average and an intermediate surface (halfway between pial and white matter boundaries) extracted for each hemisphere using marching cubes with the half maximum potential line as the threshold.
2. The intermediate surface is simplified by means of an edge collapsing algorithm to contain 18,000 polygons with the edge length limited from 0.1 to 0.3 mm (average edge length: 0.15 mm) using Amira (©Mercury Computer Systems, Inc.).
3. These surfaces are mapped to each subject using the same registration procedure as the mapping of the Laplacian grid.

The same surface, generated in average space, is thus mapped to each subject. This preserves, due to the regularization inherent in the registration, an inherent correspondence between vertices, as in MacDonald et al. (2000), i.e. vertex  $v$  in mouse 1 will map to vertex  $v$  in mouse 2, even if the mapping process had displaced that vertex to different points in space for each mouse.

The existence of an intermediate surface also allows for smoothing of the thickness along the cortical manifold. Some smoothing is likely to improve the ability to detect subtle differences between groups of mice (Lerch and Evans, 2005), and following the topology of the cortex provides better preservation of anatomical information than using a Gaussian kernel in volume space (Lerch and Evans, 2005; Chung et al., 2003). Here we employ diffusion smoothing using the Laplace Beltrami operator as described in Chung et al. (2003).

### Statistical analysis

The above algorithm results in a map of 9000 cortical thickness measures. Localising differences in cortical morphometry between groups of mice can thus be performed in the same massively univariate or multivariate ways as employed in human brain imaging. Here we employ independent linear models relating thickness to mouse genotype or other volumetric/behavioural phenotypes. Multiple comparisons are controlled using the False Discovery Rate (FDR) (Genovese et al., 2002), a technique which limits the number of allowed false positives within the set of results.

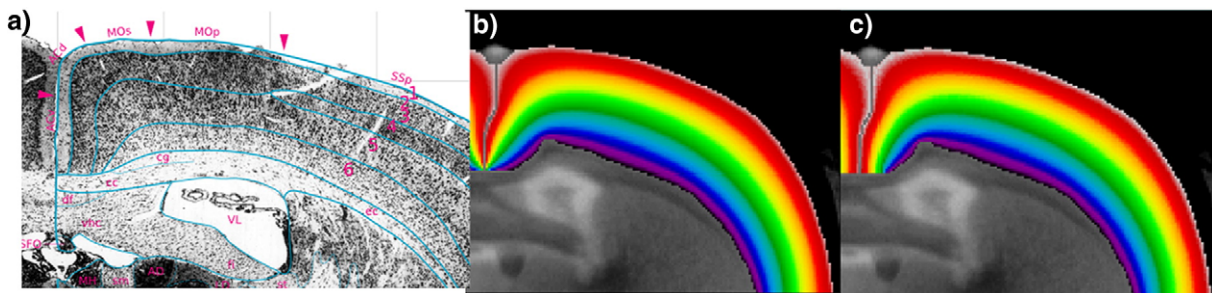


Fig. 2. Laplacian potential at the interhemispheric fissure: (a), taken from Hof et al. (2000), shows a Nissl stained slice along with anatomical annotations, including the 6 cortical layers. (b) is the Laplacian potential map using two boundaries, and (c) with the third resistive boundary added. Note how the potential lines approximate cortical layers more closely with the addition of the resistive boundary.

**Variance and power analysis**

In order to understand the cortical analysis system described herein, a group of 20 male C57BL/6 mice, first described in Spring et al. (2007), were processed. The goal was to gain an understanding of the variance inherent in the thickness and surface area measures and thus know their statistical power.

The results are shown in Fig. 3. The mean cortical thickness in these mice was 0.89 mm±0.016 mm. Given two groups of 10 mice, one can expect to recover a 0.05 mm difference in cortical thickness at α=0.005 (corresponding to a FDR of 5% in Spring et al., 2007). The shape of the power analysis graph indicates that a sufficient study size for cortical thickness analysis is around 6–9 mice per genotype.

**YAC128 mouse model**

HD is a neurodegenerative disorder characterised by motor dysfunction, psychiatric disturbances and cognitive impairment that is caused by a CAG trinucleotide expansion in the HD gene on chromosome 4 (Huntington's Collaborative Research Group, 1993). HD is classically associated with initial reduction in volume and neuronal loss primarily localised to the striatum (Vonsattel et al., 1985), but widespread brain atrophy has been described in early to mid-stage HD in humans using magnetic resonance (MR) techniques (Rosas et al., 2003).

The YAC128 mouse model of HD expresses the entire human huntingtin (htt) gene with 120 CAG repeats (Slow et al., 2003). This mouse model recapitulates many features of human HD including progressive motor and cognitive deficits, striatal and cortical atrophy with relative sparing of the hippocampus and cerebellum. These animals demonstrate low interanimal variability

(Slow et al., 2003; Van Raamsdonk et al., 2005b,a). As in human HD, the phenotype of the YAC128 mouse is progressive, with cognitive deficits detectable as early as 2 months, followed by motor deficits and specific striatal and cortical atrophy (Slow et al., 2003; Van Raamsdonk et al., 2005b). Striatal atrophy in YAC128 is associated with a decrease in neuronal count, and striatal neuronal loss at later timepoints correlates strongly with earlier motor deficits (Slow et al., 2003).

The analysis of cortical morphology presented here used the same 18 mice employed in Lerch et al. (2008). Specimen preparation and MR scanning were identical to the procedure described in Specimen preparation and MR acquisition. The cortex atlas was then mapped to each individual mouse and cortical thickness measured using the three boundary Laplacian algorithm. Thickness maps were blurred with a 0.2 mm diffusion smoothing kernel.

The analysis addressed the following questions: does the thickness of the cortex vary by genotype, does it relate to the size of the striatum, and does the relationship between cortical thickness and striatal volume differ between the wild-type and YAC128 mice. The model employed was thus the classic ANCOVA linear model:

$$\text{thickness} = \beta_0 + \beta_1 \text{Striatum} + \beta_2 \text{Genotype} + \beta_3 (\text{Genotype} \times \text{Striatum}) + \epsilon$$

where Striatum is the volume of the striatum in mm<sup>3</sup> centred on the mean striatum volume of all mice, and

$$\text{Genotype} = \begin{cases} 0 & \text{Wild type} \\ 1 & \text{YAC128} \end{cases}$$

Tests were carried out at every vertex as well as for the mean cortical thickness and overall surface area. Note that there was no correction for global brain size, as there appears to be no relationship

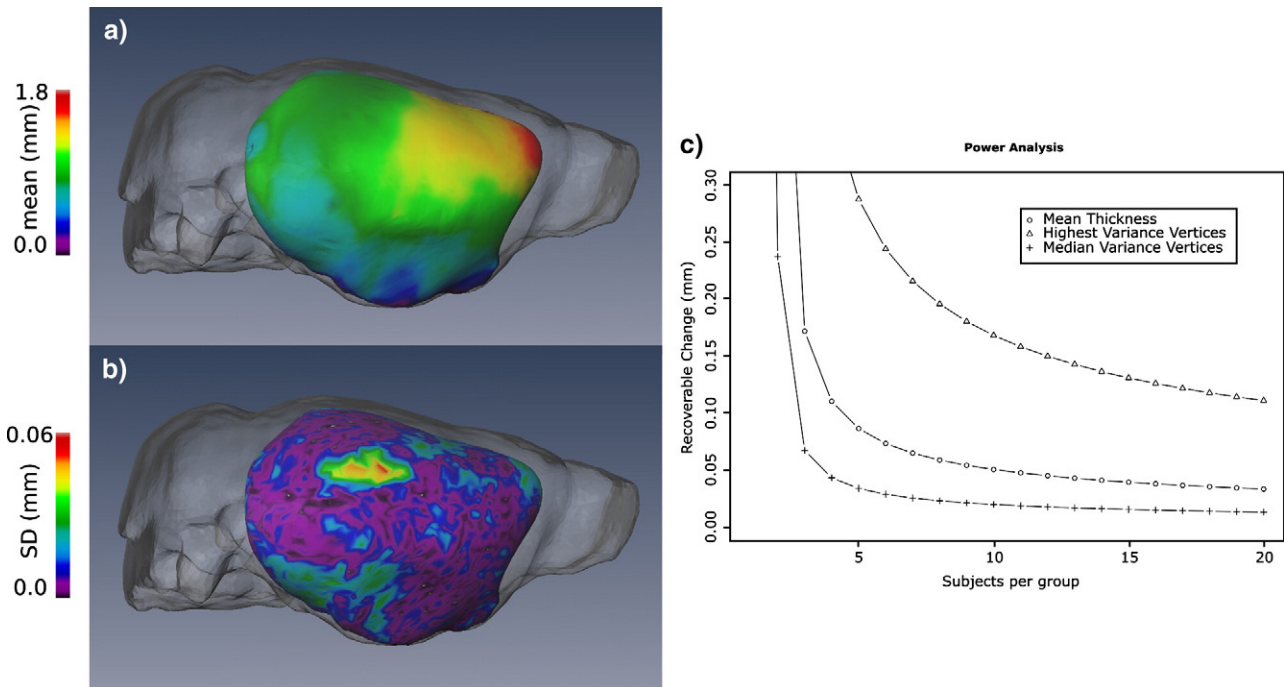


Fig. 3. Mean cortical thickness (n=20) for 12-week-old male C57BL/6 mice is shown in (a) with the standard deviation in (b). The graph in part (c) shows the expected power given two groups, the y axis specifying the recoverable change given the group sizes shown on the x axis. The three lines belong to three different estimates of standard deviation: standard deviation of mean cortical thickness (0.016 mm), the maximum variance from figure (b) (0.062 mm) and the median variance of all vertices in (b) (0.007 mm).

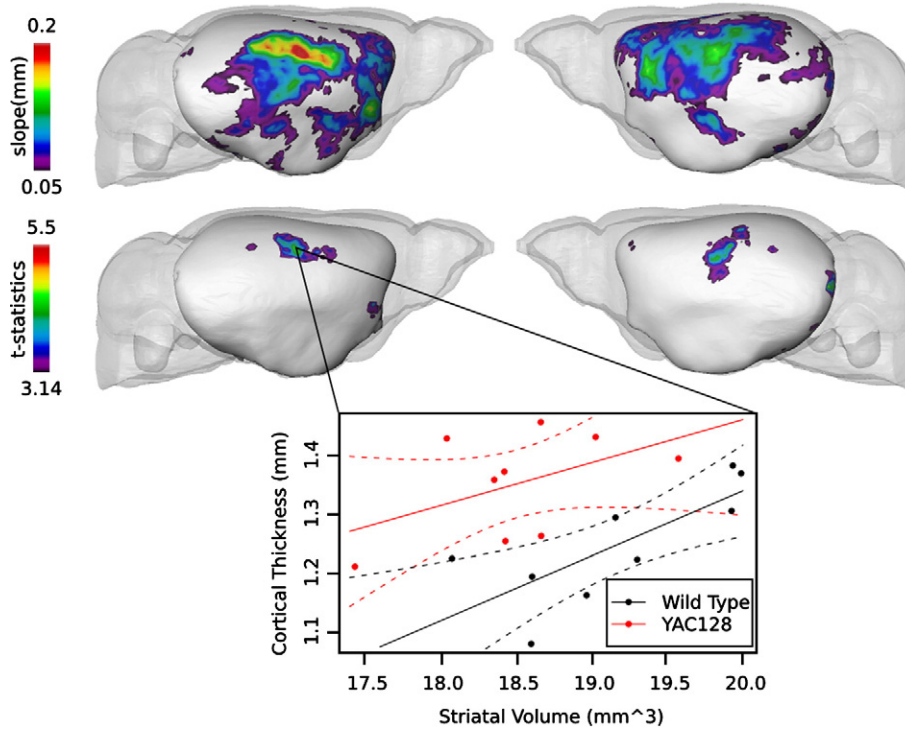


Fig. 4. Differences in overall cortical thickness between the YAC128 mouse and wild-type controls; the top row shows the difference between groups in mm, the bottom row the *t*-statistics of that difference. The sensorimotor cortex is thicker in the YAC128 mice, reaching a maximum difference of 0.19 mm. A representative vertex is plotted, the solid lines showing the linear model fit between striatal volume and cortical thickness, the dashed lines the 5% confidence interval. All effects are significant at a 10% false discovery rate.

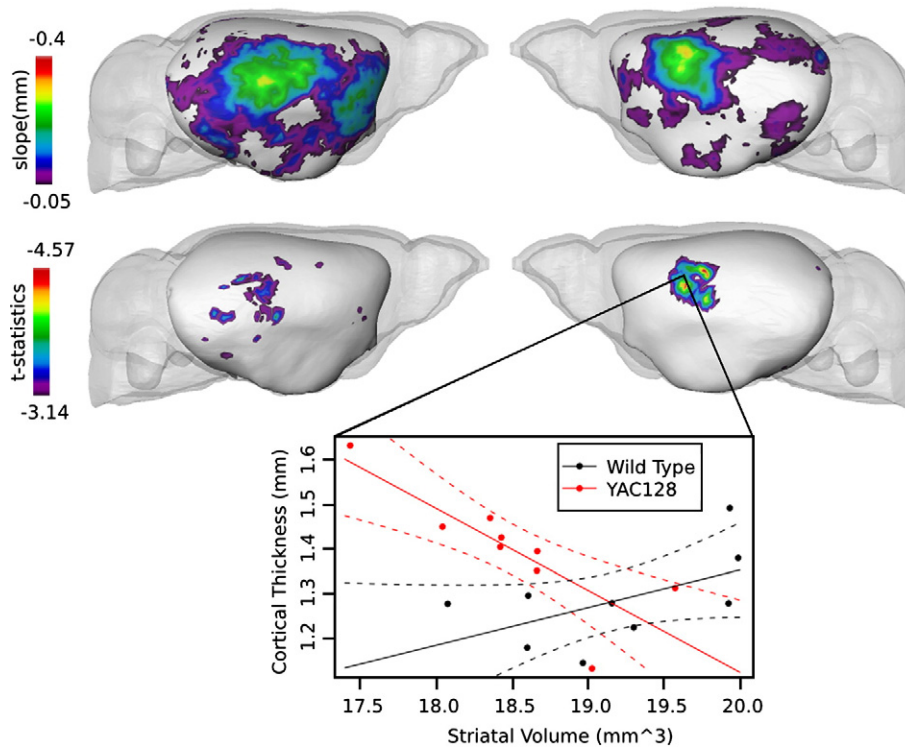


Fig. 5. Differences in the relationship between cortical thickness and striatal volume; the top row shows the difference in regression slopes in mm, the bottom row the *t*-statistics of the difference. There is a positive relationship between striatal volume and cortical thickness throughout the cortex in the wild-type mice. In the YAC128 mice, however, the sensorimotor cortex shows an inverse relationship, with cortical thickness increasing as the volume of the striatum declines. A representative vertex is plotted, solid lines representing the linear model fit and dashed lines the 5% confidence interval.

between brain size and cortical thickness. This is true in mice ( $R^2=0.01$  in the male–female data set described above) as well as humans (Luders et al., 2006).

There was a significant positive correlation between striatal volume and mean cortical thickness ( $p=0.02$ ), and the YAC128 mice had thicker cortices than wild-type controls at the centred striatal volume ( $p=0.04$ ). There was no significant interaction between striatal volume and cortical thickness. Overall surface area also correlated with striatal volume ( $p=0.01$ ), but there were no group differences nor significant interactions.

The results of the per vertex tests are shown in Figs. 4 and 5. YAC128 mice had significantly thicker sensorimotor cortices, reaching a difference of  $0.147\pm 0.04$  mm. Small increases were also found in the frontal and entorhinal cortices. Only two small regions – the anterior cingulate and the retrosplenial cortex – showed thinning in the YAC128 mice. Significant interactions between genotype and striatal volume were also found in the sensorimotor cortex, located slightly anterior to the significant group differences, wherein the wild-type mouse showed a positive correlation between striatal volume and cortical thickness while the YAC128 mice featured increasing cortical thickness with decreasing volume of the striatum.

At 8 months of age, the YAC128 mouse most closely represents a late pre-clinical or very early clinical phase of Huntington's Disease (Van Raamsdonk et al., 2005b). Motor learning deficits, as measured on the rotarod, are present as of 2 months, and cognitive function (as measured in the water maze) present at 8 months of age (Van Raamsdonk et al., 2005b), but striatal atrophy can just barely be detected (Lerch et al., 2008).

The findings of increased cortical thickness agree with previous results from human preclinical subjects (Paulsen et al., 2006). The nature of this difference is uncertain; the three most likely possibilities are a compensatory response to striatal degeneration, indications of abnormal cortical development, or some type of inflammatory response preceding cell death in later stages of the disease. Longitudinal data or more timepoints are needed in order to adequately provide a mechanism for this increase in cortical thickness; based on human data, however, it is expected that in later stages of the disease the cortex in the HD mice will indeed be thinner than their wild-type counterparts (Rosas et al., 2002), and the YAC128 mouse model has indeed been shown to have reduced cortical volume at 12 months of age (Slow et al., 2003; Van Raamsdonk et al., 2005a).

The fact that, in the sensorimotor cortex, there is an inverse correlation between striatal volume and cortical thickness only in the YAC128 mice indicates that this could indeed be a compensatory response. A recent study using functional MRI showed increasing neuronal recruitment in early HD patients using a Simon task, which tests response times under conditions of spatial incompatibility between stimulus and response (Georgiou-Karistianis et al., 2007). More importantly, that same study showed that increased activation corresponded to worsening motor deficits (Georgiou-Karistianis et al., 2007), and a previous PET study further showed increased blood flow in Huntington's patients in the parietal lobes during a triggered finger opposition task (Bartenstein et al., 1997). Increasing damage to the striatum could thus cause increasing compensatory recruitment of cortical areas (Georgiou-Karistianis et al., 2007; Paulsen et al., 2004).

## Conclusions

Here we have presented an automated algorithm for measuring cortical thickness at every point of the cortex from mouse MRI. This technique can greatly compliment the existing set of tools for

analysing differences in image deformations by providing a more biologically relevant index of cortical change. The application to the YAC128 mouse model of Huntington's Disease showed an increase in cortical thickness in response to striatal degeneration, a potential compensatory response also seen in human prodromal HD. Together these findings reaffirm the potential utility of MRI in monitoring mouse models of neurodegenerative diseases and underline the striking parallels to human HD exhibited by the YAC128 mouse.

## Acknowledgments

The authors would like to thank Dr. Claude Lepage of the Montreal Neurological Institute for valuable fixes to the code. This work was supported by grants from the Michael Smith Foundation for Health Research, the Canadian Institutes of Health Research, the Huntington's Disease Society of America and the High Q Foundation. J.P.L. is supported by the Canadian institutes for Health Research. J.B.C. is supported by the Huntington Society of Canada. M.R.H. is supported by the Canadian Institutes of Health Research, the Huntington Society of Canada, the Hereditary Disease Foundation and the Canadian Genetic Diseases Network. M.R.H. is a Killam University Professor and holds a Canada Research Chair in Human Genetics. The Mouse Imaging Centre (MICe) acknowledges funding from the Canada Foundation for Innovation and the Ontario Innovation Trust for providing facilities along with The Hospital for Sick Children. Operating funds from the Burroughs Wellcome Fund, the Canadian Institutes of Health Research, the National Cancer Institute of Canada Terry Fox Program Projects, the National Institutes of Health and the Ontario Research and Development Challenge Fund are gratefully acknowledged. R.M.H. holds a Canada Research Chair in Imaging. The authors would like to express their appreciation to Jean Paul Vonsattel and Elizabeth Aylward for their thoughtful suggestions.

## References

- Badea, A., Nicholls, P.J., Johnson, G.A., Wetsel, W.C., 2007. Neuroanatomical phenotypes in the reeler mouse. *NeuroImage* 34 (4), 1363–1374.
- Bartenstein, P., Weindl, A., Spiegel, S., Boecker, H., Wenzel, R., Ceballos-Baumann, A.O., Minoshima, S., Conrad, B., 1997. Central motor processing in Huntington's disease. A PET study. *Brain* 120, 1553–1567.
- Chen, X.J., Kovacevic, N., Lobaugh, N.J., Sled, J.G., Henkelman, R.M., Henderson, J.T., 2006. Neuroanatomical differences between mouse strains as shown by high-resolution 3D MRI. *NeuroImage* 29 (1), 99–105.
- Chung, M.K., Worsley, K.J., Robbins, S., Paus, T., Taylor, J., Giedd, J.N., Rapoport, J.L., Evans, A.C., 2003. Deformation-based surface morphometry applied to gray matter deformation. *NeuroImage* 18 (2), 198–213.
- Collins, D.L., Neelin, P., Peters, T.M., Evans, A.C., 1994. Automatic 3D intersubject registration of MR volumetric data in standardized Talairach space. *J. Comput. Assist. Tomogr.* 18 (2), 192–205.
- Collins, D.L., Holmes, C.J., Peters, T.M., Evans, A.C., 1995. Automatic 3D model-based neuroanatomical segmentation. *Hum. Brain Mapp.* 33, 190–208.
- Feigin, A., Ghilardi, M.F., Huang, C., Ma, Y., Carbon, M., Guttman, M., Paulsen, J.S., Ghez, C.P., Eidelberg, D., 2006. Preclinical Huntington's disease: compensatory brain responses during learning. *Ann. Neurol.* 59 (1), 53–59.
- Fischl, B., Dale, A.M., 2000. Measuring the thickness of the human cerebral cortex from magnetic resonance images. *Proc. Natl. Acad. Sci. U. S. A.* 97 (20), 11050–11055.
- Genovese, C.R., Lazar, N.A., Nichols, T., 2002. Thresholding of statistical maps in functional neuroimaging using the false discovery rate. *NeuroImage* 15 (4), 870–878.

- Georgiou-Karistianis, N., Sritharan, A., Farrow, M., Cunnington, R., Stout, J., Bradshaw, J., Churchyard, A., Brawn, T.L., Chua, P., Chiu, E., Thiruvady, D., Egan, G., 2007. Increased cortical recruitment in Huntington's disease using a Simon task. *Neuropsychologia* 45 (8), 1791–1800.
- Henkelman, R.M., Dazaj, J., Lifshitz, N., Nieman, B.J., Tsatskis, S., Lerch, J., Bishop, S., S.K., Sled, J.G., Chen, X.J., 2006. High throughput microimaging of the mouse brain. *ISMRM Proceedings*.
- Hof, P.R., Young, W.G., Bloom, F.E., Belichenko, P.V., Celio, M.R., 2000. *Comparative Cytoarchitectonic Atlas of the C57BL/6 and 129/Sv Mouse Brains*. Elsevier Science, Amsterdam.
- Huntington's Collaborative Research Group, 1993. A novel gene containing a trinucleotide repeat that is expanded and unstable on Huntington's disease chromosomes. The Huntington's Disease Collaborative Research Group. *Cell* 72 (6), 971–983.
- Jones, S.E., Buchbinder, B.R., Aharon, I., 2000. Three-dimensional mapping of cortical thickness using Laplace's equation. *Hum. Brain Mapp.* 11 (1), 12–32.
- Kim, J.S., Singh, V., Lee, J.K., Lerch, J., Ad-Dab'bagh, Y., MacDonald, D., Lee, J.M., Kim, S.I., Evans, A.C., 2005. Automated 3-D extraction and evaluation of the inner and outer cortical surfaces using a Laplacian map and partial volume effect classification. *NeuroImage* 27 (1), 210–221.
- Kovacevic, N., Henderson, J.T., Chan, E., Lifshitz, N., Bishop, J., Evans, A.C., Henkelman, R.M., Chen, X.J., 2005. A three-dimensional MRI atlas of the mouse brain with estimates of the average and variability. *Cereb. Cortex* 15 (5), 639–645.
- Lein, E.S., Hawrylycz, M.J., Ao, N., Ayres, M., Bensinger, A., Bernard, A., Boe, A.F., Boguski, M.S., Brockway, K.S., Byrnes, E.J., Chen, L., Chen, T.M., Chin, M.C., Chong, J., Crook, B.E., Czaplinska, A., Dang, C.N., Datta, S., Dee, N.R., Desaki, A.L., Desta, T., Diep, E., Dolbeare, T.A., Donelan, M.J., Dong, H.W., Dougherty, J.G., Duncan, B.J., Ebbert, A.J., Eichele, G., Estin, L.K., Faber, C., Facer, B.A., Fields, R., Fischer, S.R., Fliss, T.P., Frensley, C., Gates, S.N., Glattfelder, K.J., Halverson, K.R., Hart, M.R., Hohmann, J.G., Howell, M.P., Jeung, D.P., Johnson, R.A., Karr, P.T., Kawal, R., Kidney, J.M., Knapik, R.H., Kuan, C.L., Lake, J.H., Laramee, A.R., Larsen, K.D., Lau, C., Lemon, T.A., Liang, A.J., Liu, Y., Luong, L.T., Michaels, J., Morgan, J.J., Morgan, R.J., Mortrud, M.T., Mosqueda, N.F., Ng, L.L., Ng, R., Orta, G.J., Overly, C.C., Pak, T.H., Parry, S.E., Pathak, S.D., Pearson, O.C., Puchalski, R.B., Riley, Z.L., Rockett, H.R., Rowland, S.A., Royall, J.J., Ruiz, M.J., Sarno, N.R., Schaffnit, K., Shapovalova, N.V., Sivisay, T., Slaughterbeck, C.R., Smith, S.C., Smith, K.A., Smith, B.I., Sodt, A.J., Stewart, N.N., Stumpf, K.R., Sunkin, S.M., Sutram, M., Tam, A., Teemer, C.D., Thaller, C., Thompson, C.L., Varnan, L.R., Visel, A., Whitlock, R.M., Wohnoutka, P.E., Wolkey, C.K., Wong, V.Y., Wood, M., Yaylaoglu, M.B., Young, R.C., Youngstrom, B.L., Yuan, X.F., Zhang, B., Zwingman, T.A., Jones, A.R., 2007. Genome-wide atlas of gene expression in the adult mouse brain. *Nature* 445 (7124), 168–176.
- Lerch, J.P., Evans, A.C., 2005. Cortical thickness analysis examined through power analysis and a population simulation. *NeuroImage* 24 (1), 163–173.
- Lerch, J.P., Pruessner, J.C., Zijdenbos, A., Hampel, H., Teipel, S.J., Evans, A.C., 2005. Focal decline of cortical thickness in Alzheimer's disease identified by computational neuroanatomy. *Cereb. Cortex* 15 (7), 995–1001.
- Lerch, J.P., Carrol, J.B., Spring, S., Bertram, L.N., Schwab, C., Hayden, M.R., Henkelman, R.M., 2008. Automated deformation analysis in the YAC128 Huntington disease mouse model. *NeuroImage* 39 (1), 32–39.
- Luders, E., Narr, K.L., Thompson, P.M., Rex, D.E., Woods, R.P., Deluca, H., Jancke, L., Toga, A.W., 2006. Gender effects on cortical thickness and the influence of scaling. *Hum. Brain Mapp.* 27 (4), 314–324.
- Ma, Y., Hof, P.R., Grant, S.C., Blackband, S.J., Bennett, R., Slatest, L., McGuigan, M.D., Benveniste, H., 2005. A three-dimensional digital atlas database of the adult C57BL/6J mouse brain by magnetic resonance microscopy. *Neuroscience* 135 (4), 1203–1215.
- MacDonald, D., Kabani, N., Avis, D., Evans, A.C., 2000. Automated 3-D extraction of inner and outer surfaces of cerebral cortex from MRI. *NeuroImage* 12 (3), 340–356.
- Meyer, J.R., Roychowdhury, S., Russell, E.J., Callahan, C., Gitelman, D., Mesulam, M.M., 1996. Location of the central sulcus via cortical thickness of the precentral and postcentral gyri on MR. *AJNR Am. J. Neuroradiol.* 17 (9), 1699–1706.
- Miller, M.I., Massie, A.B., Ratnanather, J.T., Botteron, K.N., Csernansky, J.G., 2000. Bayesian construction of geometrically based cortical thickness metrics. *NeuroImage* 12 (6), 676–687.
- Paulsen, J.S., Zimelman, J.L., Hinton, S.C., Langbehn, D.R., Leveroni, C.L., Benjamin, M.L., Reynolds, N.C., Rao, S.M., 2004. fMRI biomarker of early neuronal dysfunction in presymptomatic Huntington's disease. *AJNR Am. J. Neuroradiol.* 25 (10), 1715–1721.
- Paulsen, J.S., Magnotta, V.A., Mikos, A.E., Paulson, H.L., Penziner, E., Andreasen, N.C., Nopoulos, P.C., 2006. Brain structure in preclinical Huntington's disease. *Biol. Psychiatry* 59 (1), 57–63.
- Paxinos, G., Franklin, K., 2001. *The Mouse Brain in Stereotaxic Coordinates*, 2nd ed. Academic Press, San Diego.
- Pitiot, A., Pausova, Z., Prior, M., Perrin, J., Loyse, N., Paus, T., 2007. Magnetic resonance imaging as a tool for in vivo and ex vivo anatomical phenotyping in experimental genetic models. *Hum. Brain Mapp.* 28 (6), 555–566.
- Preul, C., Lohmann, G., Hund-Georgiadis, M., Guthke, T., von Cramon, D.Y., 2005. Morphometry demonstrates loss of cortical thickness in cerebral microangiopathy. *J. Neurol.* 252 (4), 441–447.
- Rosas, H.D., Liu, A.K., Hersch, S., Glessner, M., Ferrante, R.J., Salat, D.H., van der Kouwe, A., Jenkins, B.G., Dale, A.M., Fischl, B., 2002. Regional and progressive thinning of the cortical ribbon in Huntington's disease. *Neurology* 58 (5), 695–701.
- Rosas, H.D., Koroshetz, W.J., Chen, Y.I., Skeuse, C., Vangel, M., Cudkovicz, M.E., Caplan, K., Marek, K., Seidman, L.J., Makris, N., Jenkins, B.G., Goldstein, J.M., 2003. Evidence for more widespread cerebral pathology in early HD: an MRI-based morphometric analysis. *Neurology* 60 (10), 1615–1620.
- Ross, M.E., Swanson, K., Dobyns, W.B., 2001. Lissencephaly with cerebellar hypoplasia (LCH): a heterogeneous group of cortical malformations. *Neuropediatrics* 32 (5), 256–263.
- Salat, D.H., Buckner, R.L., Snyder, A.Z., Greve, D.N., Desikan, R.S., Busa, E., Morris, J.C., Dale, A.M., Fischl, B., 2004. Thinning of the cerebral cortex in aging. *Cereb. Cortex* 14 (7), 721–730.
- Shaw, P., Greenstein, D., Lerch, J., Clasen, L., Lenroot, R., Gogtay, N., Evans, A., Rapoport, J., Giedd, J., 2006a. Intellectual ability and cortical development in children and adolescents. *Nature* 440 (7084), 676–679.
- Shaw, P., Lerch, J., Greenstein, D., Sharp, W., Clasen, L., Evans, A., Giedd, J., Castellanos, F.X., Rapoport, J., 2006b. Longitudinal mapping of cortical thickness and clinical outcome in children and adolescents with attention-deficit/hyperactivity disorder. *Arch. Gen. Psychiatry* 63 (5), 540–549.
- Sidman, R.L., Angevin, J.B., Pierce, E.T., 1971. *Atlas of the Mouse Brain and Spinal Cord*. Harvard University Press, Cambridge.
- Slow, E.J., van Raamsdonk, J., Rogers, D., Coleman, S.H., Graham, R.K., Deng, Y., Oh, R., Bissada, N., Hossain, S.M., Yang, Y.Z., Li, X.J., Simpson, E.M., Gutekunst, C.A., Leavitt, B.R., Hayden, M.R., 2003. Selective striatal neuronal loss in a YAC128 mouse model of Huntington disease. *Hum. Mol. Genet.* 12 (13), 1555–1567.
- Sowell, E.R., Thompson, P.M., Leonard, C.M., Welcome, S.E., Kan, E., Toga, A.W., 2004. Longitudinal mapping of cortical thickness and brain growth in normal children. *J. Neurosci.* 24 (38), 8223–8231.
- Spring, S., Lerch, J.P., Henkelman, R.M., 2007. Sexual dimorphism revealed in the structure of the mouse brain using three-dimensional magnetic resonance imaging. *NeuroImage* 35 (4), 1424–1433.
- Thompson, P.M., Dutton, R.A., Hayashi, K.M., Toga, A.W., Lopez, O.L., Aizenstein, H.J., Becker, J.T., 2005. Thinning of the cerebral cortex visualized in HIV/AIDS reflects CD4+ T lymphocyte decline. *Proc. Natl. Acad. Sci. U. S. A.* 102 (43), 15647–15652.
- Tyszka, J.M., Readhead, C., Bearer, E.L., Pautler, R.G., Jacobs, R.E., 2006. Statistical diffusion tensor histology reveals regional dysmyelination effects in the shiverer mouse mutant. *NeuroImage* 29 (4), 1058–1065.
- Van Raamsdonk, J.M., Murphy, Z., Slow, E.J., Leavitt, B.R., Hayden, M.R., 2005a. Selective degeneration and nuclear localization of mutant

- huntingtin in the YAC128 mouse model of Huntington disease. *Hum. Mol. Genet.* 14 (24), 3823–3835.
- Van Raamsdonk, J.M., Pearson, J., Slow, E.J., Hossain, S.M., Leavitt, B.R., Hayden, M.R., 2005b. Cognitive dysfunction precedes neuropathology and motor abnormalities in the YAC128 mouse model of Huntington's disease. *J. Neurosci.* 25 (16), 4169–4180.
- Vonsattel, J.P., Myers, R.H., Stevens, T.J., Ferrante, R.J., Bird, E.D., Richardson Jr., E.P., 1985. Neuropathological classification of Huntington's disease. *J. Neuropathol. Exp. Neurol.* 44 (6), 559–577.
- Walhovd, K.B., Fjell, A.M., Dale, A.M., Fischl, B., Quinn, B.T., Makris, N., Salat, D., Reinvang, I., 2006. Regional cortical thickness matters in recall after months more than minutes. *NeuroImage* 31 (3), 1343–1351.